Environment-dependent tight-binding model for molybdenum

H. Haas
Max-Planck-Institut für Metallforschung, Heisenbergstrasse 1, D-70569 Stuttgart, Germany

C. Z. Wang
Ames Laboratory and Department of Physics, Iowa State University, Ames, Iowa 50011

M. Fähnle
Max-Planck-Institut für Metallforschung, Heisenbergstrasse 1, D-70569 Stuttgart, Germany

C. Elsässer
Max-Planck-Institut für Metallforschung, Seestrasse 92, D-70174 Stuttgart, Germany

K. M. Ho
Ames Laboratory and Department of Physics, Iowa State University, Ames, Iowa 50011
(Received 4 August 1997)

A transferable orthogonal tight-binding model is developed for molybdenum, with special emphasis on applications in molecular-dynamics studies. The elements of the Hamiltonian matrix and the repulsive potential are allowed to depend on the environment in order to account for the effects of the neglected three-center matrix elements, for the neglected nonorthogonality effects and for the variation of the finite set of basis orbitals in different configurations as well. To check the accuracy of the model, the structural energy differences, the elastic constants, the phonon spectrum along high-symmetry lines in the Brillouin zone, the formation and migration energy of a vacancy, the formation energy of an octahedral interstitial atom, surface energies, and relaxations, as well as reconstructions of a (100) surface, are calculated and compared with *ab initio* data and experimental results. [S0163-1829(98)05503-9]

I. INTRODUCTION

In materials science it is often indispensable to study very large systems with a complicated structure. In spite of the enormous progress of the very accurate self-consistent *ab initio* calculations based on the density-functional theory in local-density approximation,[1] the application of this method to problems in materials science is still limited because of the enormous computational burden. On the other hand, atomistic simulations based on classical interatomic potentials often cannot give a reliable account for the quantum-mechanical aspects of bonding. Therefore, it is often attempted to establish approaches which are computationally less demanding than the density-functional calculations but which are able to describe approximately the quantum-mechanical aspects. Examples are the effective-medium theory[2] and the related embedded-atom method,[3] the density-dependent effective pair potentials derived from pseudopotential perturbation theory for simple metals[4] and for transition metals,[5] and the variety of empirical and semiempirical tight-binding (TB) methods (see, for instance, Refs. 6–8). In the latter class of methods, a Hamiltonian matrix for localized atomlike orbitals is used, and the matrix elements are not evaluated exactly, but represented in an approximate and parametrized analytical form, the parameters being determined by fitting to an appropriate set of experimental or theoretical data. These TB methods are particularly suited to incorporate covalency effects and to determine not only total energies and forces, but also the relevant electronic features like the electronic band structure, the density of states,[9] and the bond order, which are extremely useful for an interpretation of the bonding properties. The interest in TB methods has increased recently because of the development of O(N) (or linear scaling) algorithms (see, for instance, Ref. 10) for calculating the total energy and forces with a computational effort which scales linearly with the number N of atoms in the system (whereas most of the conventional self-consistent band structure methods scale like N^3). All of these algorithms rely on the truncation of quantum correlations in real space, making the TB description a natural framework for such algorithms. The dramatic increase (at least 10 times) in the size of the system that is accessible by an O(N) TB molecular-dynamics scheme opens up new classes of problems that can now be investigated. Furthermore, it allows[7,11] for a systematic many-body expansion of the bond order in terms of the moments of the density of states, where the lowest-order (i.e., second-order) approximation is mathematically identical to the Finnis-Sinclair potential.[12]

The success of the TB methods depends on whether an appropriate parametrization of the TB Hamiltonian can be found which allows for an accurate fit to the experimental or theoretical input data for selected configurations and which is transferable to other configurations to be investigated. The original domain of TB methods was the description of strongly covalent solids with special emphasis on Si and C (see, for instance, Refs. 13–15). The application to metals is probably more demanding: In simple metals the s and p electrons are delocalized and a TB approach does not appear

to be the most natural approach, and in transition metals there is a coexistence of delocalized *s* and *p* electrons and more localized *d* electrons. Nevertheless, it turned out[7] that many gross features of transition metals may be correctly described by TB models which involve only the *d* electrons. A simple orthogonal *d*-band model for the energy and forces in Mo was suggested by Paxton.[16] To account for more subtle effects, however, *s*, *p*, and *d* states have to be considered. Mehl and Papaconstantopoulos[17] developed a two-center nonorthogonal TB method with intra-atomic Hamiltonian matrix elements which depend on the local environment and with the parameters fitted to *ab initio* band-structure and total energy data, and they applied this general scheme to 29 of the alkaline earth metals, transition metals (including Mo), and noble metals. Varma and Weber[18] developed an excellent nonorthogonal *s*-*p*-*d* model for the calculation of phonon frequencies in Mo, which, however, is tailored for a determination of the dynamical matrix (for instance, some contributions to the dynamical matrix are fitted to the phonon spectrum) and cannot be used directly for a total energy and force calculation. One of the objectives of the present paper is to consider just one transition metal, namely, Mo, and to develop a TB model for this metal which is as accurate as possible to explore how far we can go with a TB description of this metal. In our model, special emphasis will be given to the dependence of the matrix elements and the pair potential on the environment, very much in the sense of the method developed by Tang *et al.*[15] for C. The second objective of the present paper is to develop this model in such a way that it is suitable for molecular-dynamics simulations. The general scheme of Mehl and Papaconstantopoulos[17] involves interactions to neighbors within a sphere of radius 16.5 a.u. Depending on the structure and the lattice constant, this sphere includes from 80 to 300 neighboring atoms, which constitutes a very large computational effort for molecular-dynamics simulations. We will confine ourselves to interactions up to typically at most third-nearest-neighbor interactions.

In Sec. II we describe the theoretical basis for our TB model, whose parameters are determined by fitting to an appropriate set of data which are obtained mainly from *ab initio* electron theory. In Sec. III we discuss the results of our model for the cohesive properties, the properties of vacancies and interstitials, for phonons as well as energies, relaxations, and reconstructions of surfaces, and a concluding discussion is given in Sec. IV.

II. CALCULATIONAL METHOD

A. TB band model

The starting point for the systematic derivation of TB models (and for the effective-medium theory and the embedded-atom model) is the Harris-Foulkes functional,[19,20] which allows a reliable estimate of the total energy without performing a self-consistent density-functional band-structure calculation,

$$E=\sum_i f_i\epsilon_i^{\rm out}-\frac{e^2}{2}\int\frac{\rho^{\rm in}(\mathbf{r})\rho^{\rm in}(\mathbf{r}')}{|\mathbf{r}-\mathbf{r}'|}\,d^3r\,d^3r'+\int\rho^{\rm in}(\mathbf{r})\times\{\epsilon_{\rm xc}[\rho^{\rm in}]-V_{\rm xc}[\rho^{\rm in}]\}d^3r+\frac{e^2}{2}\sum_{\alpha,\alpha'\neq\alpha}\frac{Z_\alpha Z_{\alpha'}}{|\mathbf{R}_\alpha-\mathbf{R}_{\alpha'}|}. \quad (1)$$

Here Z_α and $Z_{\alpha'}$ are the charges of ionic cores at sites $\mathbf{R}_\alpha$ and $\mathbf{R}_{\alpha'}$. $\rho^{\rm in}$ is the input valence charge density, i.e., an appropriate *Ansatz* for the real charge density, and $V_{\rm xc}[\rho^{\rm in}]$ and $\epsilon_{\rm xc}[\rho^{\rm in}]$ are the functionals[1] of the exchange-correlation potential and the exchange-correlation energy per electron. The eigenvalues $\epsilon_i^{\rm out}$ are to be obtained from the solution of the Kohn-Sham equations[1]

$$\left\{-\frac{\hbar^2}{2m}\Delta+V_{\rm eff}(r)\right\}\varphi_i(\mathbf{r})=\epsilon_i\varphi_i(\mathbf{r}) \quad (2)$$

for the single-particle eigenfunctions $\varphi_i(\mathbf{r})$, with the effective potential

$$V_{\rm eff}(\mathbf{r})=V(\mathbf{r})+V_H[\rho^{\rm in}(\mathbf{r})]+V_{\rm xc}[\rho^{\rm in}(\mathbf{r})], \quad (3)$$

where V and V_H denote the Coulomb potential of the ionic cores and the Hartree potential. The f_i are the occupation numbers.

The TB model may be derived from Eq. (1) by inserting a superposition of atomic charge densities $\rho_\alpha(|\mathbf{r}-\mathbf{R}_\alpha|)$,

$$\rho^{\rm in}(\mathbf{r})=\sum_\alpha\rho_\alpha(|\mathbf{r}-\mathbf{R}_\alpha|), \quad (4)$$

for the input charge density $\rho^{\rm in}$, i.e., by neglecting the bond-charge density, which is justified for strongly localized states. Truncating the many-body expansion of the nonlinear functionals $\epsilon_{\rm xc}[\rho^{\rm in}]$ and $V_{\rm xc}[\rho^{\rm in}]$ after the pair-potential term and omitting terms which do not depend on the structure, the total energy may be written[19] in the form

$$E^{\rm TB}=\sum_i f_i\epsilon_i^{\rm out}+\sum_{\alpha,\alpha'\neq\alpha}\phi(r_{\alpha,\alpha'}), \quad (5)$$

with pair potentials $\phi(r_{\alpha,\alpha'})$ which depend only on the interatomic distance $r_{\alpha,\alpha'}=|\mathbf{R}_\alpha-\mathbf{R}_{\alpha'}|$ and with eigenvalues $\epsilon_i^{\rm out}$ determined via Eq. (2) with an effective potential constructed from the TB charge density (4).

Equation (5) is the basis for most TB band models (Mehl and Papaconstoupoulos[17] have shown that a TB model can also be formulated without resort to a pair-potential term). The approximations involved are (i) the lack of self-consistency, (ii) the neglect of the bond-charge density in the *Ansatz* for $\rho^{\rm in}$, and (iii) the neglect of many-body contributions from $\epsilon_{\rm xc}$ and $V_{\rm xc}$.

It should be noted that the theory may be reformulated by regrouping various terms in the total energy to obtain the so-called TB bond model (see, for instance, Ref. 8) which allows for an approximate account of self-consistency in the total energy calculation via the physically motivated constraint that in most metallic systems the atoms are nearly charge neutral. In the TB band model which we use, there is no explicit account for self-consistency effects.

B. Orthogonal two-center TB approximation

The Kohn-Sham equation (2) may be solved by expanding $\varphi_i(\mathbf{r})$ into a set of atomiclike orbitals $|\alpha p\rangle$ attached at the atoms α (p is an index characterizing the orbitals),

$$\varphi_i(\mathbf{r}) = |\varphi_i\rangle = \sum_{\alpha p} C^i_{\alpha p} |\alpha p\rangle, \tag{6}$$

yielding the set of equations

$$\sum_{\alpha p} H_{\alpha' p', \alpha p} C^i_{\alpha p} = \epsilon_i \sum_{\alpha p} S_{\alpha' p', \alpha p} C^i_{\alpha p}, \tag{7}$$

with the Hamiltonian matrix $H_{\alpha' p', \alpha p} = \langle \alpha' p' | \hat{\mathbf{H}} | \alpha p \rangle$, the overlap matrix $S_{\alpha' p', \alpha p} = \langle \alpha' p' | \alpha p \rangle$, and the Hamiltonian $\hat{\mathbf{H}} = -(\hbar^2/2m)\Delta + V_{\text{eff}}(\mathbf{r})$. Instead of calculating the Hamiltonian and overlap matrix for some explicitly given basis set $|\alpha p\rangle$, we perform a semiempirical approach by making appropriate analytical *Ansätze* with open parameters which are fitted to an appropriate set of data mainly from *ab initio* calculations. We thereby adopt the following approximations.

(a) Use of a minimal basis set, i.e., instead of working with a complete set of basis functions, we consider a minimal basis set of atom-centered localized orbitals with just one orbital for each angular and magnetic quantum number. For different atomic configurations the degree of completeness of this minimal basis set is also different, which affects the transferability of the TB model. This problem may be cured in part by the use of environment-dependent Hamiltonian matrix elements (see below).

(b) Orthogonal TB method, i.e., we deal with a diagonal overlap matrix. This may be conceived in two alternative ways. First, we can argue that we deal implicitly with orthogonalized, i.e., Löwdin-transformed atomiclike orbitals.[21] Then the overlap matrix is indeed diagonal. The disadvantage of this concept is that Löwdin orbitals are often not very well localized so that we come in conflict with the TB approximation for the Hamiltonian matrix; see point (c). Confining ourselves nevertheless to a small number of near-neighbor matrix elements then would deteriorate the transferability of the TB model to different configurations. Second, we can argue that we deal implicitly with nonorthogonal basis functions. Harrison[6] has shown that the neglect of the nondiagonal overlap matrix elements may be repaired by a shift of the interatomic matrix elements and by a shift of the average single-particle energies ϵ_i^{out}. When fitting the Hamiltonian matrix elements to an *ab initio* band structure, the shift of the interatomic matrix elements is automatically accounted for. The shift of the average ϵ_i^{out} may be approximately absorbed[6] into the pair-potential term and then is again included when fitting to *ab initio* data. The disadvantage of this concept is that the physical meaning of the pair-potential term is more and more obscured. The approximations involved in an orthogonal method may be corrected in part by the use of environment-dependent Hamiltonian matrix elements (see below).

(c) TB approximation for the Hamiltonian matrix elements. Because of the implicit use of localized atomiclike basis orbitals, we set $H_{\alpha' p', \alpha p} = 0$ for $r_{\alpha\alpha'} > r_{\text{cutoff}}$. In the present paper we choose the cutoff radius in such a way that for the bcc ground state matrix elements up to at most third-nearest neighbors are included.

(d) Two-center approximation. Using the *Ansatz* (4) for the density and neglecting the nonlinearity of V_{xc}, the effective potential may be written in the form

$$V_{\text{eff}}(\mathbf{r}) = \sum_{\alpha} V_{\text{eff},\alpha}(|\mathbf{r} - \mathbf{R}_\alpha), \tag{8}$$

yielding

$$H_{\alpha' p', \alpha p} = \langle \alpha' p' | -\frac{\hbar^2}{2m}\Delta + \sum_{\alpha''} V_{\text{eff},\alpha''} | \alpha p \rangle. \tag{9}$$

In the following we distinguish between three types of matrix elements.

(1) Three-center terms $\alpha \neq \alpha' \neq \alpha''$. Because of the implicitly assumed small spatial extension of the basis orbitals, these terms are neglected in a two-center approximation.

(2) Interatomic two-center matrix elements $\langle \alpha' p' | V_{\text{eff},\alpha} + V_{\text{eff},\alpha'} | \alpha p \rangle$. If the orbital index p stands for angular and magnetic quantum numbers, these interatomic two-center matrix elements may be represented[6] as linear combinations of Slater-Koster elements $V_{ll'm}$ (only matrix elements between orbitals with the same magnetic quantum number survive), the coefficients being determined exclusively by the orientation of the atom pair α, α' in the crystal. For an elementary metal there are ten independent Slater-Koster elements when including s, p, and d states. In the traditional two-center approximation, the Slater-Koster elements $V_{ll'm}$ depend only on the distance between the sites $\mathbf{R}_\alpha$ and $\mathbf{R}_{\alpha'}$. In the present model, we extend this to include a dependence on the environment of the atoms α and α'.

(3) Intra-atomic matrix elements $\alpha = \alpha'$. For an elementary metal there are three intraatomic matrix elements (ϵ_s, ϵ_p, and ϵ_d) whose environment dependence is taken into account by $\epsilon_d = \epsilon_d^0 + \Sigma_{\alpha''} \Delta\epsilon_d(r_{\alpha\alpha''})$, $\epsilon_s = \epsilon_d + \epsilon_{s\text{-}d}^0 + \Sigma_{\alpha''} \Delta\epsilon_{s\text{-}d}(r_{\alpha\alpha''})$ and an analogous equation for ϵ_p. Here the quantities with superscript 0 denote the parts independent of the environment and the $\Delta\epsilon_l$ are the environment-dependent contributions. In the present model, all matrix elements with $p \neq p'$ are neglected.

C. Parametrization of the Hamiltonian matrix

According to Sec. II B, we must find an appropriate parametrization for ten Slater-Koster elements $V_{ll'm}$, respectively, the intraatomic terms and the pair potential $\phi(r_{\alpha\alpha'})$. We thereby assume that $V_{ll'm}$, $\Delta\epsilon_l$, and $\phi(r_{\alpha\alpha'})$ are environment dependent. The environment dependence of $\Delta\epsilon_l$ becomes obvious from Sec. II B. Concerning the Slater-Koster elements, the following situation appears: If we try to fit independently nearest-neighbor and next-nearest-neighbor Slater-Koster elements V^1 and V^2 as a function of the lattice constant a of the bcc crystal to an *ab initio* band structure (Sec. II D), we obtain a gap between V^1 and V^2 especially for the $V_{ss\sigma}$ elements which cannot be described by a parametrization for which the Slater-Koster elements depend exclusively and smoothly on the distance. There are at least two reasons for this gap: First, when we fit to an *ab initio* band structure, we formally arrive at environment-dependent two-center elements, although these do not depend explicitly on the environment (see Sec. II B) because we have neglected three-center matrix elements. Second, we have argued in Sec. II B that the use of an orthogonal method may be conceived as working implicitly with Löwdin orbitals which may be obtained by a Löwdin transformation of origi-

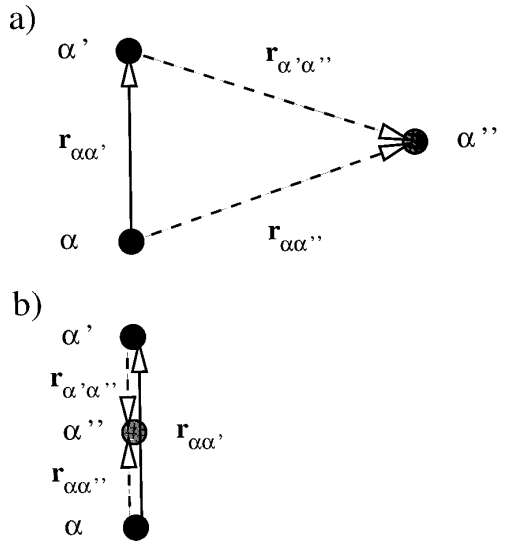

FIG. 1. Arrangement of atoms used in the text to illuminate the effects of the screening function.

nally nonorthogonal atomiclike orbitals. However, the two-center Hamiltonian matrix elements of the Löwdin orbitals then depend on the structural configuration, although the original two-center Hamiltonian matrix elements do not. In the following we therefore will allow for a dependence of the Hamiltonian matrix elements on the environment. We thereby hope that this will also help to cure part of the problems arising from the use of an incomplete minimal basis set [point (a) of Sec. II B]. Concerning the pair potential, a contribution to the environment dependence may arise from the neglect of the many-body terms of $\epsilon_{\rm xc}$ and $V_{\rm xc}$ (Sec. II B), and another contribution may arise from that part of the pair potential which accounts for the neglect of the nondiagonal overlap matrix elements (Sec. II B).

In the following we adopt the same functional form for the distance dependence of $V_{ll'm}$, $\Delta\epsilon_l$, and $\phi(r_{\alpha\alpha'})$, namely,

$$f(r_{\alpha\alpha'})=C_1\,\exp(-C_2 r_{\alpha\alpha'})(1-S_{\alpha\alpha'}); \tag{10}$$

i.e., the primary distance dependence is given by the exponential and the environment dependence is modeled by the screening function introduced by Tang *et al.*,[15]

$$S_{\alpha\alpha'}=\tanh 2\xi_{\alpha\alpha'}\,, \tag{11}$$

$$\xi_{\alpha\alpha'}=C_3\sum_{\alpha''}\exp\left(-C_4\,\frac{r_{\alpha\alpha''}+r_{\alpha'\alpha''}}{r_{\alpha\alpha'}}\right)^{C_5}. \tag{12}$$

There are 5 parameters C_i (with $C_2\cdots C_5>0$) for the 14 functions $V_{ll'm}$ (10), $\Delta\epsilon_l$ (3), and ϕ (1), and the 3 parameters ϵ_l, so that, altogether, the model would contain 73 parameters.

The meaning of the screening function for the value of $f(r_{\alpha\alpha'})$ is discussed for the two atomic arrangements shown in Fig. 1. Figure 1(a) represents a situation where the atom α'' is far from the line connecting the atoms α and α'. In this situation we have a large value of $(r_{\alpha\alpha''}+r_{\alpha'\alpha''})/r_{\alpha\alpha'}$, and hence $\xi_{\alpha\alpha'}$ and $S_{\alpha\alpha'}$ are small so that there is nearly no screening of the exponential in Eq. (10). In contrast, if α'' is on the midpoint of the line connecting α and α' [Fig. 1(b)], then $(r_{\alpha\alpha''}+r_{\alpha'\alpha''})/r_{\alpha\alpha'}$ is 1, $\xi_{\alpha\alpha'}$ and $S_{\alpha\alpha'}$ may be larger (depending on the parameters C_3, C_4, and C_5) and there may be an appreciable screening of the exponential in Eq. (10). It will become apparent from Fig. 4 that the above-discussed gap between the first- and second-nearest-neighbor Slater-Koster elements is naturally obtained by the use of the screening procedure. It should be noted that an environment-dependent parametrization was also suggested by other authors. Mehl and Papaconstantopoulos[17] as well as Mercer and Chou[22] used environment-dependent intraatomic matrix elements. Andriotis[23] introduced a dependence of the matrix elements on the local coordination numbers. Serra *et al.*[24] did not use environment-dependent matrix elements, but they introduced an environment-dependent correction term for the whole band-structure part of Eq. (5) based on suitably defined local coordination numbers as well as a corresponding correction term for the pair-potential part.

All interactions in our model are truncated at a cutoff radius of 8.9 a.u. Depending on the structure and the lattice constant, this means that in all our investigated systems up to typically third-nearest-neighbor interactions are included so that the computational effort for molecular-dynamics simulations remains moderate. Because of the screening of the interatomic matrix elements, these are automatically rather short ranged so that we do not need an explicit cutoff function to shorten the interaction range.

D. Determination of the parameters

We first reduced the actual number of parameters used for the fits by imposing for the preexponential factors the universal ratios[6] $V_{pd\sigma}:V_{pd\pi}=-\sqrt{3}:1$ and $V_{dd\sigma}:V_{dd\pi}:V_{dd\delta}=(-6):4:(-1)$ for all interaction shells, saving altogether 15 parameters. Furthermore, we realized from the fits that $V_{pp\pi}$ is small and can be neglected without a noticeable change of the results, saving 5 more parameters (actually $V_{pp\pi}$ is not smaller than part of the dd-matrix elements which we keep, but the occupied bands are mainly of d character and therefore the neglect of $V_{pp\pi}$ does not matter much). We thus end up with altogether 53 parameters, which are yet to be determined. This large number of fit parameters contributes a big computational problem, because the fit function certainly exhibits a large number of local minima and it is nearly impossible to find numerically the absolute minimum. Starting from different initial values of the parameters will most probably yield fit parameters corresponding to different minima. Concerning this problem, we agree with the statement given in the paper of Cohen *et al.*[25] ''Great care is needed to test the resulting model for reasonable behavior outside the range of the fit.'' This care may be taken in different ways. First, we can exclude all those models which yield unreasonable results for such configurations outside the range of the fit and try to find another model related to another minimum of the fit function which yields reasonable results. Second, we can include additional configurations in the fit which are close to the configurations to be investigated, hoping that then our fitting procedure yields automatically a more adequate minimum of the fit function. We will proceed on the second line.

In a first attempt we proceeded along the line of Tang *et al.*[15] for C: i.e., we determined the parameters by a fit to

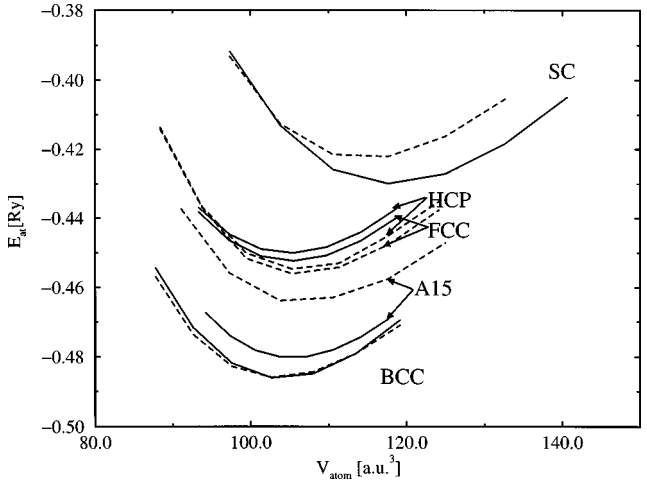

FIG. 2. Total energy vs volume for sc, bcc, fcc, and hcp Mo and for Mo in the A15 structure. The dashed and solid lines represent the TB and *ab initio* LMTO-ASA data, respectively.

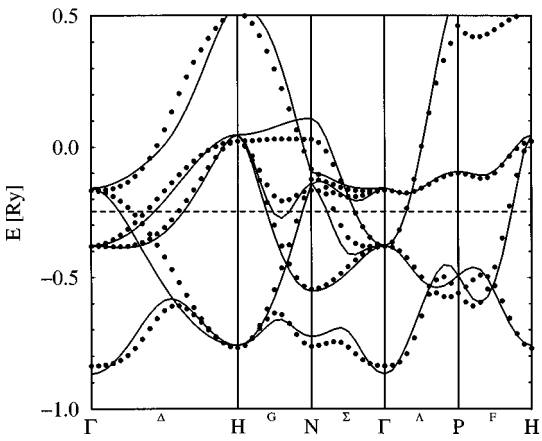

FIG. 3. TB band structure (dots) of bcc Mo at $a_0 = 5.8$ a.u. in comparison with the *ab initio* LMTO-ASA band structure (solid lines).

ab initio data for the band structure along lines of high symmetry in the Brillouin zone and the total energy for Mo in various crystal structures (sc, bcc, fcc) and for a variety of lattice parameters around the respective equilibrium lattice parameters (we omitted the structures with low coordination numbers, i.e., linear chain and graphite or diamond structure, which are important for covalent materials, but not for transition metals). All the *ab initio* calculations are performed using the linear-muffin-tin-orbital method in atomic-sphere approximation[26] (LMTO-ASA). It should be emphasized that we fit *simultaneously* to data from band structure and total energy. Alternatively, we could first fit the matrix elements to the band structure and then the pair potential to the total energy. This, however, would restrict the variational degree for the fit, and it would be somehow inconsistent because the neglect of the off-diagonal elements of the overlap matrix affects both the band structure and the pair potential (see Sec. II B).

It turned out that the so-obtained TB model yields unsatisfactory results, for instance, for the vacancy formation energy, for some phonon dispersion branches, for the elastic constant C_{44}, and for the energies and relaxations of surfaces. We therefore included additional data in the database for the fitting procedure. Our hope is that by including more than just a minimal set of fit configurations the self-consistency effects which are neglected explicitly in the present model are taken into account implicitly: If we managed to correctly describe all conceivable fit configurations, the model would implicitly include the self-consistency effects. To be specific, we have included the following informations.

(i) The experimental phonon frequencies at the points N,H,P of the phonon Brillouin zone. We used the experimental data because the *ab initio* data depart[27,28] from the experimental results.

(ii) The experimentally obtained elastic constant C_{44}.

(iii) The vacancy formation energy obtained[29] by the mixed-basis pseudopotential (MBPP) method[30–33] for an unrelaxed supercell with 16 sites and one vacancy.

(iv) The unrelaxed (100) surface energy obtained[34] by the MBPP method.

(v) Information on the surface relaxation. It was observed experimentally[35] that the topmost surface layer of molybdenum exhibits an inward relaxation of about 10%. It would be extremely time consuming if we obtained for each set of 53 parameters the actual surface relaxation of the tight-binding model defined by these parameters and then included the deviation of the calculated and the experimentally observed relaxation into the database for the fitting procedure. Instead, we calculated the total energy for a system for which nine

TABLE I. Values of the 53 independent parameters of our TB model.

	C_1 [Ry]	C_2 [a.u.$^{-1}$]	C_3	C_4	C_5
$V_{ss\sigma}$	−1.96039	0.49567	0.91879	0.32609	3.29680
$V_{pp\sigma}$	0.15126	0.00335	1.72287	0.57285	4.40026
$V_{dd\sigma}$	−4.28813	0.75383	1.22539	2.06345	1.88137
$V_{sp\sigma}$	0.21139	0.10603	0.14827	0.00823	9.43875
$V_{sd\sigma}$	−0.58079	0.43117	20.40798	0.51628	12.40635
$V_{pd\sigma}$	−4.20194	0.79336	19.34963	0.50985	12.35016
$\Delta\epsilon_{s\text{-}d}$	3.04032	0.79552	56.12257	1.25854	4.33453
$\Delta\epsilon_{p\text{-}d}$	1.94008	0.69334	19.41967	0.92420	3.53797
$\Delta\epsilon_d$	−0.05986	0.62099	14.80478	0.62766	3.73126
ϕ	350.43775	1.73214	14.07585	0.86263	3.14150

$\epsilon^0_{s\text{-}d} = 0.03738$Ry, $\epsilon^0_{p\text{-}d} = 0.26068$ Ry, $\epsilon^0_d = 0.08304$ Ry

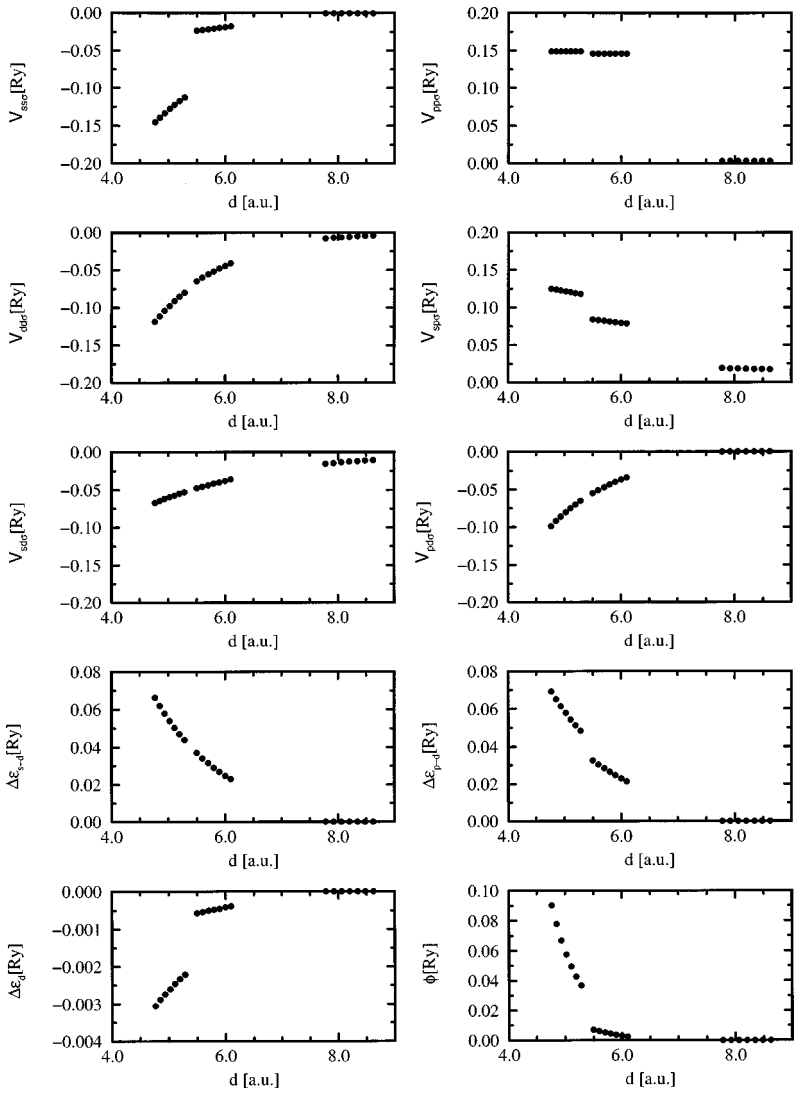

FIG. 4. Dependences of the independent Slater-Koster elements $V_{ll'm}$, of the intra-atomic parameters $\Delta\epsilon$, and of the pair potential ϕ, on the interatomic distance d.

(100) layers and a vacuum space corresponding to three layers are repeated periodically, with the topmost layer relaxed inwards by 20%, i.e., twice the experimental value. Implying a parabolic dependence of the total energy on the degree of inward relaxation of the topmost layer with a minimum at 10% relaxation, the energy of this system should be the same as the one of a corresponding unrelaxed system; i.e., we include this energy difference in the database for the fitting procedure.

To asses the quality of the fits, Fig. 2 shows the fitted total energy curves for sc, bcc, and fcc Mo and Fig. 3 exhibits the fitted curves to the band structure in bcc Mo. Please note that for changes in the binding properties due to deviations from the ideal structure (phonons, defects, etc.) mainly the energies close to the Fermi energy are relevant. In addition, Fig. 2 includes data for Mo in hcp and A15 structure, which were not used for the fit. It becomes obvious that the TB results agree well with the *ab initio* results for the hcp structure, but not for the A15 structure, which indicates limitations of the transferability of our model.

The final values of the 53 parameters defining our model are given in Table I, and the distance dependences of the independent Slater-Koster parameters and of the intra-atomic parameters and of ϕ are shown in Fig. 4. Please note the discontinuity in the interaction parameters, for instance, between the first- and second-nearest neighbors, which in our model is a natural consequence of the screening explained in Sec. II C and Fig. 1.

Because the distance dependences of the Hamiltonian matrix elements and the pair potential are given in analytical form, the forces on the atom γ can be readily calculated via $\mathbf{F}_\gamma = -\nabla_\gamma E^{\mathrm{TB}}(\{\mathbf{R}_\alpha\})$ (using the Hellmann-Feynman theorem[36] for the band-structure part) and used for the static relaxation of atoms or for molecular-dynamics studies.

III. RESULTS

In this section we will briefly report on some results of our TB calculations in order to demonstrate the capability and the limitations of the model. A more extensive discussion concerning the TB molecular-dynamics simulations for phonons at zero and finite temperature or of the surface relaxations and reconstructions will be given elsewhere.

TABLE II. Results of the TB model for the equilibrium lattice constant a_0, the elastic constants C_{11}, C_{12}, and C_{44}, the vacancy formation energy E_V^f, and the formation energy E_I^f of an octahedral interstitial atom in a relaxed supercell containing 16 sites, in comparison with results from *ab initio* MBPP calculations and experimental data.

	a_0 [a.u.]	C_{11} [Mbar]	C_{12} [Mbar]	C_{44} [Mbar]	E_V^f [eV]	E_I^f [eV]
TB	5.912	4.10 ± 0.10	1.82 ± 0.10	1.24 ± 0.04	3.11	10.40
MBPP	5.926[a]				2.90 ± 0.1[a]	9.54[b]
Experiment	5.945[c]	4.50[d]	1.73[d]	1.25[d]	2.9[e]	

[a]Reference 29.
[b]Reference 40.
[c]Reference 37.
[d]Reference 38.
[e]Reference 39.

A. Bulk properties

Table II represents the TB results for bcc Mo for the equilibrium lattice constant a_0, the elastic constant C_{11}, C_{12}, and C_{44}, the vacancy formation energy E_V^f for a relaxed supercell with 54 sites, and the formation energy E_I^f for an octahedral interstitial atom in a relaxed supercell with 16 regular lattice sites, in comparison with experimental results and with results from the MBPP approach. The quantities a_0 and C_{44} were included in the fit, and therefore the comparison simply tests for the quality of the fit. In contrast, the results for C_{11}, and C_{12}, for E_V^f in the relaxed supercell, and for E_I^f are predictions of the TB model, which agree rather well with the data from experiments (C_{11},C_{12},E_V^f) and/or the MBPP calculation (E_V^f,E_I^f). For E_V^f the agreement with experiments and the MBPP method is excellent. It thereby should be noted that the agreement with the MBPP method for the unrelaxed supercells is worse: In the TB model (MBPP calculation) the energy gain due to the relaxation (structural relaxation of the atoms around the vacancy and volume relaxation of the supercell after introduction of a vacancy) is 0.5 eV (0.16 eV). For the interstitial atom on the octahedral site, there are very short interatomic distances. Therefore, this configuration is different from any configuration used for the fit, and the good agreement between the TB result and the MBPP result is astonishing. To reduce the computational effort (for the MBPP method), we used a small supercell for comparison. To obtain realistic values for E_I^f for comparison with experiments, much larger supercells had to be considered. Again, the agreement between the TB and MBPP results is much worse for the unrelaxed interstitial configuration (where the interatomic distances are even smaller), for which the TB value for E_I^f is nearly twice the MBPP value, although the relaxational displacements of the atoms obtained by the methods are rather similar.

Figure 5 exhibits the total energy as function of the displacement of an atom along $\langle 111\rangle$ into a nearest-neighbor vacancy in an unrelaxed supercell with 16 sites. A double-peak structure of the total energy similar to the one obtained by Tsai *et al.*[41] for Fe via pair-potential calculations is found both in the TB model and in the MBPP study.

Figure 6 exhibits the TB results for the phonon frequencies at zero temperature as obtained by a dynamical-matrix approach (see, for instance, Ref. 42) and by frozen-phonon calculations (see, for instance, Ref. 43). In the dynamical-matrix approach anharmonicities are accounted for as in Ref. 42. In the frozen-phonon calculations we fitted for the high-symmetry points in the Brillouin zone the energy versus displacement data by a polynomial $E=a\delta^2+b\delta^4+c\delta^6$ and calculated the phonon frequency from the coefficient a. Alternatively and for intermediate points on high-symmetry lines, we performed the frozen-phonon calculation for one single but small displacement $\delta=0.01a_0$ for which we assumed that the harmonic approximation holds. The validity of this assumption was confirmed by test calculations with an even smaller displacement of $\delta=0.001a_0$ and by the good agreement of the so-obtained frequencies with those from the polynomial fit at high-symmetry points. The calculations are converged with respect to the number of k points used for the sampling of the electronic Brillouin zone, except for the H point (for the problems involved in the calculation of the H point phonon in Mo, see, for instance, Ref. 28). From Fig. 6 it becomes obvious that there are small discrepancies between the results from the dynamical-matrix approach and the frozen-phonon approach, because of the following reason:[42] In the frozen-phonon calculations all conceivable

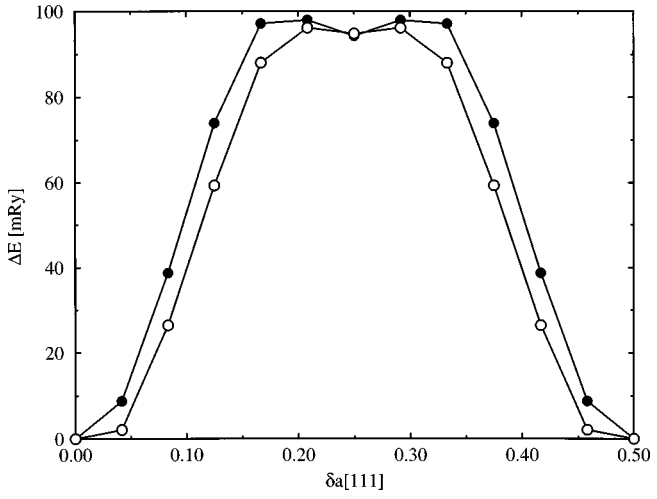

FIG. 5. Increase of the total energy per supercell as function of the displacement of an atom along $\langle 111\rangle$ into a nearest-neighbor vacancy in bcc Mo (unrelaxed supercell with 16 sites). Open circles, TB; solid dots, *ab initio* MBPP.

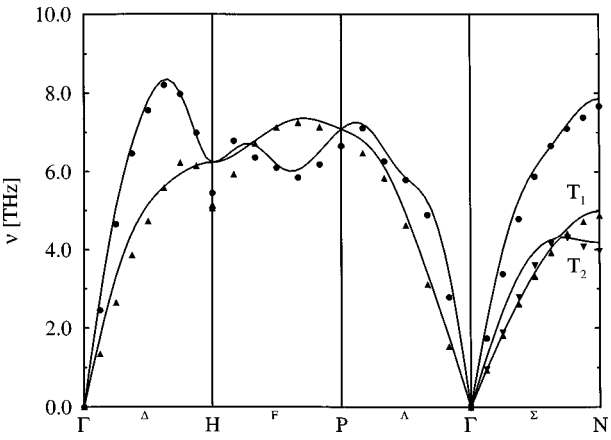

FIG. 6. TB results for the phonon branches of bcc Mo along high-symmetry lines. Solid lines: dynamical-matrix method. Dots (longitudinal modes) and triangles (transversal modes): frozen-phonon calculation.

couplings between the atoms are accounted for exactly, whereas in the supercell calculations of the dynamical matrix the long-range couplings are affected by finite-size effects. Whereas in Na and K, for instance, it is sufficient to take into account couplings up to the third-nearest-neighbor shell,[42] in Mo couplings up to a much larger range have to be considered[44] to obtain an accurate phonon spectrum. The supercell containing 250 atoms which we used in our calculations of the dynamical matrix obviously is not large enough. In Fig. 7 we therefore compare the more reliable data from frozen-phonon calculations with the experimental results obtained[44] by inelastic neutron scattering at 296 K. In spite of some quantitative discrepancies, the qualitative agreement is satisfactory: The most important phonon anomalies in Mo, i.e., the low frequency of the H point phonon, the lowering of the T_2 mode when approaching the N point along the Σ line, and the crossing of the longitudinal and the transversal phonon branches along the F line, are correctly reproduced by the TB model.

As mentioned in the Introduction, it was our concern to develop a transferable TB model for applications in molecular dynamics. To demonstrate the feasibility of such calculations based on our TB model, we performed a microcanonical molecular dynamics study for $T=10$ K for a box containing 54 atoms and determined the phonon frequencies from the Fourier transform of the velocity correlation function. The results agreed very well with those obtained from frozen-phonon calculations for a supercell with 54 atoms when using the same number of k points for the sampling of the electronic Brillouin zone. In a future publication we will report on our TB molecular-dynamics study of phonons at elevated temperatures which were performed to see whether the present model is able to reproduce the shifts of the phonon frequencies with temperature observed[45] by inelastic neutron scattering.

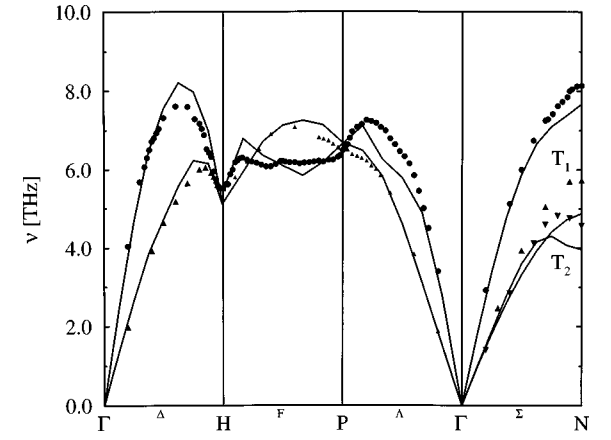

FIG. 7. Comparison of the phonon frequencies in bcc Mo from the TB method (frozen-phonon calculation, solid lines) and from inelastic neutron scattering (Ref. 44) at $T=296$ K (dots).

TABLE III. Relaxation of the $p(1\times1)$ (100) surface. Δd_{12} is the relative change of the interlayer distance (in percent) between the first and second layers compared to the interlayer distance in the bulk. n_S represents the number of atomic planes in the supercell.

	MBPP[a]	TB		
	$n_S=7$	$n_S=7$	$n_S=9$	$n_S=11$
Δd_{12}	−10.7	−8.7	−11.0	−11.9
Δd_{23}	+2.7	+3.0	+4.3	+5.1
Δd_{34}	+0.3	−1.5	−2.7	−3.4
Δd_{45}			+0.3	+1.2
Δd_{56}				−0.6

[a]Reference 34.

B. Surface properties

As mentioned in Sec. II D, we included information on the (100) surface properties in the database for the fitting procedure. Thereby the results for the bulk are only slightly affected, whereas the inclusion is really essential for the treatment of the surface: When we did not include these data for the fitting procedure, we arrived at (100) and (110) surface energies which were about 25% too small, and at an inward relaxation of the topmost (100) layer which was twice the relaxation found in *ab initio* calculations and in experiments. When including the (100) surface energy in the fit, we obtained good results (see below) for the surface energies of both the (100) and (110) surfaces.

We investigated the $p(1\times1)$ relaxation of the (100) surface, i.e., the inward or outward relaxation of the planes near an unreconstructed (100) surface, for supercells containing slabs with $N_s=7$, 9, and 11 planes and a vacuum space corresponding to 3 layers separating the slabs (Table III). The results for the relaxations were rather well converged with respect to the number of k points: Doubling the number of k points in the irreducible part of the Brillouin zone changed the results by less than 5%. For the two outermost layers our results agree quite well with those obtained by a MBPP calculation[34] for $N_s=7$, and with the experimental values for the relaxation of the topmost layer obtained by low-energy electron-diffraction (LEED) experiments, which yield an inward relaxation of (9.5 ± 2)% (Ref. 35) or 11.5% (Ref. 46).

Concerning the surface reconstruction, we found that the (100) surface is stable with respect to displacements according to a M_1-surface phonon mode, but unstable with respect to an M_5-surface phonon mode, in agreement with MBPP calculations.[34] A comparison between the TB and MBPP re-

TABLE IV. Relaxation and $(\sqrt{2}\times\sqrt{2})45°$ reconstruction of the (100) surface. Δd_{12} has the same meaning as in Table III. The quantities δ_i denote the displacements (in percent of the net constant for the reconstruction, 8.361 a.u.) of the atoms in the ith plane parallel to the surface along the surface ⟨11⟩ direction. N_S represents the number of atomic planes in the supercell.

	MBPP[a]	TB		
	$n_S=7$	$n_S=7$	$n_S=9$	$n_S=11$
Δd_{12}	−7.9	−6.6	−6.9	−7.8
Δd_{23}	+1.2	+1.4	+2.1	+2.5
Δd_{34}	+0.3	−1.1	−1.4	−2.1
Δd_{45}			−0.1	+0.6
Δd_{56}				−0.3
δ_1	4.8	5.5	5.2	4.8
δ_2	0.4	1.9	1.7	1.6
δ_3	−0.1	0.6	0.4	0.4
δ_4	∼0.0	0.5	0.3	0.2
δ_5			0.2	∼0.0
δ_6				∼0.0

[a]Reference 34.

sults for the relaxation and reconstruction data of the resulting $(\sqrt{2}\times\sqrt{2})45°$ surface is given in Table IV. Future calculations with larger supercells are required in order to find out whether the model is also able to yield the experimentally observed $(7\sqrt{2}\times\sqrt{2})45°$ reconstruction (see, for instance, Ref. 47). The surface energies for the (100) surface are given in Table V. The results agree very well with the MBPP data of Wang *et al.*[34] For the surface energy of an unrelaxed and nonreconstructed (110) surface, our TB model with $n_s=7$ yields a value of 1.38 eV per surface atom. Including relaxation of the topmost layer, a full-potential-LMTO calculation[48] with $n_s=7$ obtained a value of 1.34 eV per surface atom.

Finally, we have calculated the local density of electronic states for the layers near the surface. In agreement with full-potential linearized-augmented-plane-wave calculations[49] we found that for the surface layer the Fermi energy is located in a sharp peak of the electronic density of states, whereas in the bulk it is located in a pseudogap.

IV. DISCUSSION

We have developed a highly transferable orthogonal two-center TB model for Mo with special emphasis on the applicability in molecular-dynamics studies. The key ingredients are as follows.

(i) The matrix elements and the pair potential depend on the environment in order to account implicitly for the effects of the neglected three-center matrix elements, for the nonorthogonality effects, and for the variation of the finite set of basis orbitals in different configurations as well. Altogether, the model contains 53 fit parameters.

(ii) The large number of fit parameters makes the model flexible enough for a fit to many experimental data and/or data from *ab initio* calculations for various strongly differing atomic configurations. The hope is that thereby self-consistency effects which are not explicitly accounted for in the model are implicitly taken into account. On the other hand, the large number of fit parameters constitutes a serious mathematical problem because of the large number of local minima of the fit function. Therefore, the model has to be tested carefully for configurations outside the range of the fit.

TABLE V. Surface energies (in eV per surface atom) for an unrelaxed, relaxed, and $(\sqrt{2}\times\sqrt{2})45°$-reconstructed (100) plane.

n_S		$p(1\times1)$ Unrelaxed	$p(1\times1)$ Relaxed	$(\sqrt{2}\times\sqrt{2})45°$ Relaxed
7	MBPP[a]	2.18	2.07	2.056
7	TB	2.198	2.110	2.069
9	TB	2.193	2.086	2.070
11	TB	2.181	2.056	2.052

[a]Reference 34.

The transferability of the model has been tested for such configurations which were not explicitly included in the fit (cohesive energies for special structures, phonon spectrum, energy of formation and migration of a vacancy, formation energy of an interstitial atom, surface relaxations and surface reconstructions, surface energies). In most cases the quantitative agreement between the TB results and the data from *ab initio* calculations and/or experiments was satisfactory or even very good. Nevertheless, there are a few cases for which the agreement is not yet really satisfactory. For instance, the TB result for the cohesive energy of Mo in the A15 structure deviates much more from the *ab initio* data than the results for the other crystal structures. Another example is the tendency of our model to overestimate the effects of structural relaxation: For the vacancy and especially for the interstitial atom, our relaxation energies are much larger than the corresponding *ab initio* data, and without explicitly including in the fitting procedure some information on the relaxation near the surface the TB model would arrive at a far too strong surface relaxation. We think that the explicit neglect of self-consistency effects might be responsible for the problems of the model to describe the relaxation effects correctly as long as no information at all on the relaxation properties for the considered configuration is included in the fitting procedure.

Altogether, we think that in spite of the good overall transferability of the developed TB model, still great care is needed when applying the model to other situations: For many problems in materials science, the TB model is required to circumvent the tough restrictions for the system sizes imposed when working with *ab initio* methods. To assure the transferability of our TB model to new situations, we then suggest to test the model first for small system sizes against *ab initio* calculations. If the transferability is confirmed, then the model is extremely useful for considering the sometimes very large system sizes required in materials science.

ACKNOWLEDGMENT

One of the authors (H.H.) acknowledges financial support from the Deutscher Akademischer Austauschdienst.

[1] W. Kohn and L. J. Sham, Phys. Rev. **140**, A1133 (1965).
[2] N. Chetty, K. Stokbro, K. W. Jacobsen, and J. K. Nørskov, Phys. Rev. B **46**, 3798 (1992).
[3] M. S. Daw and M. I. Baskes, Phys. Rev. Lett. **50**, 1285 (1983).
[4] J. Hafner, *From Hamiltonians to Phase Diagrams*, Springer Series in Solid-State Sciences Vol. 70 (Springer, Berlin, 1987).
[5] J. A. Moriarty, Phys. Rev. B **42**, 1609 (1990).
[6] W. A. Harrison, *Electronic Structure and the Properties of Solids* (Dover, New York, 1989).
[7] D. Pettifor, *Bonding and Structure of Molecules and Solids* (Clarendon, Oxford, 1995).
[8] A. P. Sutton, M. W. Finnis, D. G. Pettifor, and Y. Ohta, J. Phys. C **21**, 35 (1988).
[9] H. Haas, C. Elsässer, and M. Fähnle, J. Phys.: Condens. Matter **8**, 10 353 (1996).
[10] D. G. Pettifor and D. L. Weaire, *The Recursion Method and Its Applications* (Springer, Berlin, 1995).
[11] A. P. Horsfield, A. M. Bratkosky, D. G. Pettifor, and M. Aoki, Phys. Rev. B **53**, 1656 (1996).
[12] M. W. Finnis and J. E. Sinclair, Philos. Mag. A **50**, 45 (1984).
[13] D. J. Chadi, Phys. Rev. Lett. **41**, 1062 (1978); **59**, 1691 (1988); Phys. Rev. B **29**, 785 (1984).
[14] L. Goodwin, A. J. Skinner, and D. G. Pettifor, Europhys. Lett. **9**, 701 (1989).
[15] M. S. Tang, C. Z. Wang, C. T. Chan, and K. M. Ho, Phys. Rev. B **53**, 979 (1996).
[16] A. T. Paxton, J. Phys. D **29**, 1689 (1996).
[17] M. J. Mehl and D. A. Papaconstantopoulos, Phys. Rev. B **54**, 4519 (1996).
[18] C. M. Varma and W. Weber, Phys. Rev. Lett. **39**, 1094 (1977).
[19] J. Harris, Phys. Rev. B **31**, 1770 (1985).
[20] W. M. C. Foulkes, Ph.D. thesis, University of Cambridge, 1987; W. M. C. Foulkes and R. Haydock, Phys. Rev. B **39**, 12 520 (1989).
[21] P.-O. Löwdin, J. Chem. Phys. **18**, 365 (1950).
[22] J. L. Mercer, Jr. and M. Y. Chou, Phys. Rev. B **49**, 8506 (1994).
[23] A. N. Andriotis, J. Phys.: Condens. Matter **7**, L61 (1995).
[24] S. Serra, C. Molteni, and L. Miglio, J. Phys.: Condens. Matter **7**, 4019 (1995).
[25] R. E. Cohen, M. J. Mehl, and D. A. Papaconstantopoulos, Phys. Rev. B **50**, 14 694 (1994).
[26] O. K. Andersen and O. Jepsen, Phys. Rev. Lett. **53**, 2571 (1984).
[27] K. M. Ho, C. L. Fu, B. N. Harmon, W. Weber, and D. R. Hamann, Phys. Rev. Lett. **49**, 673 (1982).
[28] S. Buck, K. Hummler, and M. Fähnle, Phys. Status Solidi B **195**, K9 (1996).
[29] B. Meyer and M. Fähnle, Phys. Rev. **56**, 13 595 (1997).
[30] S. G. Louie, K. M. Ho, and M. L. Cohen, Phys. Rev. B **19**, 1774 (1979).
[31] C.-L. Fu and K. M. Ho, Phys. Rev. B **28**, 5480 (1983).
[32] C. Elsässer, N. Takeuchi, K. M. Ho, C.-T. Chan, P. Braun, and M. Fähnle, J. Phys.: Condens. Matter **2**, 4371 (1990).
[33] K. M. Ho, C. Elsässer, C.-T. Chan, and M. Fähnle, J. Phys.: Condens. Matter **4**, 5189 (1992).
[34] X. W. Wang, C. T. Chan, K. M. Ho, and W. Weber, Phys. Rev. Lett. **60**, 2066 (1988).
[35] L. J. Clarke, Surf. Sci. **91**, 131 (1980).
[36] H. Hellmann, *Einführung in die Quantenchemie* (Deuticke, Leipzig, 1937); R. P. Feynman, Phys. Rev. **56**, 340 (1939).
[37] Y. Waseda, K. Hirata, and M. Ohtani, High Temp.-High Press. **7**, 221 (1975).
[38] F. H. Featherston and J. R. Neighbours, Phys. Rev. **130**, 1324 (1963).
[39] R. Ziegler and H.-E. Schaefer, Mater. Sci. Forum **15–18**, 145 (1987).
[40] B. Meyer (private communication).
[41] D. H. Tsai, R. Bullough, and R. C. Perrin, J. Phys. C **3**, 2022 (1970).
[42] W. Frank, U. Breier, C. Elsässer, and M. Fähnle, Phys. Rev. Lett. **77**, 518 (1996).
[43] K. Kunc, in *Electronic Structure Dynamics and Quantum Structured Properties of Condensed Matter*, edited by D. T. Devreese and P. van Camp (Plenum, New York, 1985), p. 227.
[44] B. M. Powell, P. Martel, and A. D. B. Woods, Can. J. Phys. **55**, 1601 (1977).
[45] J. Zarestky, C. Stassis, B. N. Harmon, K. M. Ho, and C. L. Fu, Phys. Rev. B **28**, 697 (1983).
[46] A. Ignatiev, F. Jona, H. D. Shih, D. W. Jepsen, and P. M. Marcus, Phys. Rev. B **11**, 4787 (1975).
[47] E. Hulpke and D. M. Smilgies, Phys. Rev. B **43**, 1260 (1991).
[48] M. Methfessel, D. Hennig, and M. Scheffler, Phys. Rev. B **46**, 4816 (1992).
[49] S. C. Hong and J. I. Lee, in *International Conference on the Physics of Transition Metals*, edited by P. M. Oppeneer and F. Kübler (World Scientific, Singapore, 1992), p. 524.